Progress In Electromagnetics Research, Vol. 142, 771–798, 2013

POLARIZATION-AGILE ADS-INTERLEAVED PLANAR ARRAYS

Giacomo Oliveri, Leonardo Lizzi, Fabrizio Robol, and Andrea Massa*

ELEDIA Research Center, Department of Information Engineering and Computer Science, University of Trento, Via Sommarive 5, Trento 38123, Italy

Abstract—This paper presents a class of polarization-agile arrays with controlled sidelobes. The architecture is based on the interleaving of two independently polarized sub-arrays through a deterministic strategy derived from Almost Difference Sets (ADSs). The efficiency, flexibility and reliability of the proposed design technique is assessed by means of a set of numerical simulations. Moreover, selected experiments aimed at comparing the performances of the presented approach with state-of-the-art design are provided. Finally, mutual coupling effects are numerically analyzed and discussed.

1. INTRODUCTION

Polarization-reconfigurable arrays play a fundamental role in modern wireless [1, 2] and radar systems [3–6] since they allow an enhancement of their discrimination capabilities and a more significant clutter suppression. Moreover, polarization agility has been indicated as a tool for reducing glint errors in tracking radars [7], as well as to mitigate multi-path fading in wireless communication systems [6]. More recent applications of polarization agile arrays include, for example, broadband communication systems for in-flight entertainment [6].

In order to reach polarization agility, the integration of cross-polarized individual radiators in standard array configurations has been first considered [3]. Towards this end, several architectures based on actively controlled antennas [5, 8–16] have been proposed. Unfortunately, such an approach has the drawback of significantly

Received 27 July 2013, Accepted 16 September 2013, Scheduled 18 October 2013

* Corresponding author: Andrea Massa (andrea.massa@unitn.it).

increasing the overall system complexity [6]. In order to mitigate this problem, architectures exhibiting a reduced beam steering [17, 18] or considering sequential rotation of the feeding [19] have been investigated [6]. However, also these approaches exhibit some limitations in terms of feeding network complexity, flexibility, or radiation properties [6].

In this framework, shared aperture architectures with orthogonal polarizations have been recently proposed for the design of polarization-agile arrays [6]. More specifically, two fully interleaved layouts [20] have been considered for the synthesis of narrow beams with arbitrary polarization states [6]. Thanks to the properties of the employed *Difference Sets* (DS)-based interleaving scheme [21], good performances in terms of polarization purity and peak sidelobe level control have been demonstrated with a simple feeding network [6].

Nevertheless, the application of such design approach is limited by the availability of a DS blueprint of the suitable dimension [22]. Indeed, DSs have the fundamental drawback that they exist (or can be designed) only for specific lengths and thinning factors [22–24]. In order to overcome this limitation while achieving satisfactory results (i.e., close to those of DSs), the utilization of sets with sub-optimal (i.e., three-level) autocorrelation properties has been proposed in the field of combinatorial mathematics [25, 26]. The so-called *Almost Difference Sets* (ADSs) [25, 26] have actually been successfully applied in several array design problems comprising thinned [27–30], interleaved [31, 32], and $MIMO$ [33] layouts. Hybrid ADS-based design methodologies have been proposed as well for wireless communications [34] and radio-astronomy applications [35].

In such a framework, ADSs appear to be good candidates for enlarging the range of applicability of the design approach proposed in [6] without a significant degradation of the obtained performances in terms of PSL control and polarization purity.

In this paper, the exploitation of ADS blueprints for the design of polarization-agile interleaved arrays is introduced. The proposed approach is aimed at synthesizing arrays with performances close to that obtained by DSs, while enlarging the set of admissible design configurations. It is worth remarking that the objective of the paper is not to synthesize optimal layouts, but rather (a) to propose simple and reliable guidelines which can be exploited when a sub-optimal but computationally efficient design tool is preferred to a stochastically optimization, and (b) to suggest a possible initialization for a global optimizer aimed at synthesizing the *optimal* architecture. Towards this end, the considered polarization-agile architecture is discussed in Section 2 along with the ADS design methodology and the expected

features. Afterwards, an extensive numerical analysis aimed at highlighting advantages and drawbacks of the proposed approach also in comparison with state-of-the-art techniques is presented (Section 3). The effects of mutual coupling on the performances of ADS-based polarization agile arrays is then assessed by means of full-wave simulations exploiting the method of moments (MoM).

2. MATHEMATICAL FORMULATION

Let us consider a planar array composed of $N = P \times Q$ equally weighted elements spaced by $s_x \times s_y$ wavelengths. Let the elements be grouped into two sub-arrays (respectively called "H" and "V" sub-arrays) of K_V and $K_H = N - K_V$ elements, and assume that each one of them contains identical elementary radiators. The far-field radiation pattern of such array, in the absence of mutual coupling, is given by [7, 36, 37]

$$\mathbf{E}(u,v) = \alpha_H \mathbf{E}_H(u,v) + \alpha_V \mathbf{E}_V(u,v) \tag{1}$$

where

$$\mathbf{E}_T(u,v) = \mathbf{EF}_T(u,v) \times AF_T(u,v) \tag{2}$$

is the field radiated by the "T" sub-array [$T = \{H,\ V\}$], and $AF_T(u,v)$ is the sub-array factor

$$AF_T(u,v) \triangleq \sum_{p=0}^{P-1} \sum_{q=0}^{Q-1} w_T(p,q) \exp\{2\pi i \left[p s_x \left(u - u_0\right) + q s_y \left(v - v_0\right)\right]\}, \tag{3}$$

$\mathbf{EF}_T(u,v)$ is the element pattern, $w_T(p,q)$ the weight of its (p,q)-th element (with $w_H(p,q) = 1 - w_V(p,q)$ and $\sum_{p=0}^{P-1} \sum_{q=0}^{Q-1} w_T(p,q) = K_T$), α_T the sub-array weight, $u = \sin(\theta)\cos(\varphi)$, $v = \sin(\theta)\sin(\varphi)$ ($u^2 + v^2 \leq 1$), and (u_0, v_0) the steering direction. Indeed, each sub-array is fed by a single amplifier, as it can be noticed by the sketch of the considered architecture [Fig. 1]. As regards the achievable polarization states, by writing $\mathbf{E}(u,v)$ in the steering direction in terms of its polar components

$$\mathbf{E}\left(u_0, v_0\right) = E^{\theta}\left(u_0, v_0\right) \hat{\theta} + E^{\varphi}\left(u_0, v_0\right) \hat{\varphi} \tag{4}$$

and using (1), it turns out that

$$\begin{cases} E^{\theta}\left(u_0, v_0\right) = \alpha_H E_H^{\theta}\left(u_0, v_0\right) + \alpha_V E_V^{\theta}\left(u_0, v_0\right) \\ E^{\varphi}\left(u_0, v_0\right) = \alpha_H E_H^{\varphi}\left(u_0, v_0\right) + \alpha_V E_V^{\varphi}\left(u_0, v_0\right) \end{cases} \tag{5}$$

where $\mathbf{E}_T\left(u_0, v_0\right) = E_T^{\theta}\left(u_0, v_0\right) \hat{\theta} + E_T^{\varphi}\left(u_0, v_0\right) \hat{\varphi}$. Solving the linear system (5) with respect to α_H and α_V, one obtain that the following

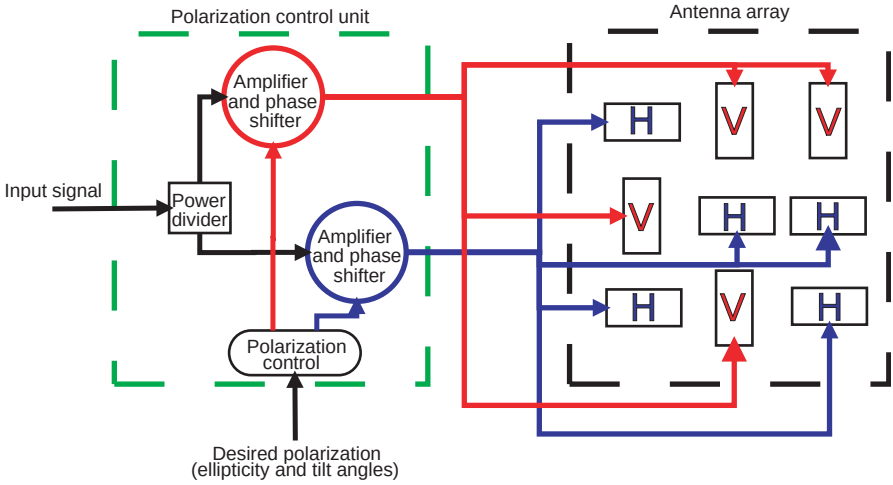

Figure 1. *Mathematical Formulation.* Layout of a polarization-agile array based on a fully-interleaved architecture. "H" and "V" denote independently polarized elements.

set of complex coefficients

$$\begin{cases} \alpha_H = \dfrac{E^{\theta}(u_0,v_0)\,E_V^{\varphi}(u_0,v_0) - E^{\varphi}(u_0,v_0)\,E_V^{\theta}(u_0,v_0)}{E_H^{\theta}(u_0,v_0)\,E_V^{\varphi}(u_0,v_0) - E_H^{\varphi}(u_0,v_0)\,E_V^{\theta}(u_0,v_0)} \\ \alpha_V = \dfrac{E_H^{\theta}(u_0,v_0)\,E^{\varphi}(u_0,v_0) - E_H^{\varphi}(u_0,v_0)\,E^{\theta}(u_0,v_0)}{E_H^{\theta}(u_0,v_0)\,E_V^{\varphi}(u_0,v_0) - E_H^{\varphi}(u_0,v_0)\,E_V^{\theta}(u_0,v_0)} \end{cases} \tag{6}$$

Eq. (6) opens the path towards obtaining arbitrary polarization states by conveniently adjusting $\{\alpha_H, \alpha_V\}$ to obtain the desired $\{E^{\theta}(u_0,v_0), E^{\varphi}(u_0,v_0)\}$, provided that $\mathbf{E}_H(u_0,v_0)$ and $\mathbf{E}_V(u_0,v_0)$ are linearly independent [otherwise, (5) cannot be inverted] [6]. This can be easily assured by considering, for example, orthogonally displaced linearly polarized elements for the two sub-arrays [6].

Although the considered architecture allows an easy control of the polarization state of the radiated wave, the same does not hold true for its peak sidelobe level [6]. Indeed, such a parameter, which is of great importance for radar and wireless system and is defined as

$$PSL \triangleq \frac{\max_{u,v \notin R}\{S(u,v)\}}{S(u_0,v_0)}, \tag{7}$$

[$S(u,v) = |\mathbf{E}(u,v)|^2$ being the total radiated power and $R^{\dagger}$ the radiation pattern mainlobe region] depends on $w_H(p,q)$ and $w_V(p,q)$.

† In the following, $R \triangleq \{(u,v) \in \mathbb{R}^2,\, u^2+v^2 \le 1, \sqrt{(u-u_0)^2+(v-u_0)^2} < \rho\}$, where $\rho \triangleq \sqrt{\frac{4}{PQs_xs_y}}$.

As a consequence, ad-hoc design techniques have to be employed in order to guarantee low *PSL* values [6].

In this paper, the application of *ADS* blueprints to the synthesis of polarization-agile interleaved arrangements is proposed. Towards this end, the sub-array aggregation for the H layout is selected as follows

$$w_H(p,q) = \begin{cases} 1 & \text{if } (p,q) \in \mathbf{A}_H \\ 0 & \text{otherwise} \end{cases} \tag{8}$$

where $\mathbf{A}_H$ is a (N, K_H, Λ_H, t)-ADS[‡], that is a set of K_H unique elements belonging to $\mathbf{G} \triangleq \mathbb{Z}^P \otimes \mathbb{Z}^Q$ (Λ_H, t being parameters which define the autocorrelation properties of the considered ADS) [25, 26]. Such a sub-array therefore is actually an ADS-based thinned array [28]. Accordingly, it can be deduced that [28]

$$\left| AF_H\left(\frac{k}{s_x P}, \frac{l}{s_y Q}\right)\right|^2 = \Xi_H(k,l) \quad k=0,\ldots,P-1,\ l=0,\ldots,Q-1 \tag{9}$$

where $\Xi_H(k,l) \triangleq \sum_{\tau_x=0}^{P-1}\sum_{\tau_y=0}^{Q-1} \xi_H(\tau_x,\tau_y)\ \exp[2\pi i(\frac{\tau_x k}{P} + \frac{\tau_y l}{Q})]$ is the inverse discrete Fourier transform ($IDFT$) of the autocorrelation function $\xi_H(\tau_x,\tau_y) \triangleq \sum_{p=0}^{P-1}\sum_{q=0}^{Q-1} w_H(p,q)\ w_H[(p+\tau_x)|_{mod\,P},\ (q+\tau_y)|_{mod\,Q}]$ ($P \times Q$ being its period), of ADS-binary sequences, i.e., the following three-level function [25, 26]

$$\xi_H(\tau_x,\tau_y) = \begin{cases} K_H & (\tau_x,\tau_y) = 0 \\ \Lambda_H & \text{for } t \text{ values of } (\tau_x,\tau_y) \\ \Lambda_H + 1 & \text{otherwise,} \end{cases}, \tag{10}$$

which, as anticipated, is very close to the two-level autocorrelation of DS sequences [26]. By using (10) and (9), one can deduce that the samples of the square amplitude of $AF_H(u,v)$ are equal to [28]

$$\Xi_H(k,l) = K_H - \Lambda_H + N\Lambda_H\,\delta(k,l) + \Psi(k,l) \tag{11}$$

where $\delta(k,l)$ is the discrete impulse function [$\delta(k,l) = 1$ if $k = l = 0$ and $\delta(k,l) = 0$, otherwise], $\Psi(k,l) \triangleq IDFT\{\psi(\tau_x,\tau_y)\}$ being $\psi(t_x,t_y) \triangleq \sum_{r=1}^{N-1-t} \delta(\tau_x - \tau_x^r, \tau_y - \tau_y^r)$, and (τ_x^r, τ_y^r), $r = 1,\ldots,N-1-t$, are the indexes at which $\xi_H(\tau_x^r,\tau_y^r) = \Lambda_H + 1$ [28].

Thanks to (9), a set of *a-priori* bounds, which applies to $AF_H(u,v)$, have been derived for the PSLs of ADS-based thinned arrays [28]. However, in order to assess the behaviour of the interleaved architecture of interest, the properties of $AF_V(u,v)$ have to be analyzed as well. Towards this end, let us consider the following theorem:

[‡] *ADS* properties, construction techniques, theorems and explicit expressions can be found in [25, 26, 43].

Theorem 1 [25] — If $\mathbf{A}_H$ is an *ADS* then its complementary set $\mathbf{A}_V \triangleq \mathbf{G}\backslash\mathbf{A}_H$, (i.e., $\mathbf{A}_V = \{(p,q) \in \mathbf{G}\text{: } (p,q) \notin \mathbf{A}_V\}$) is an (N, K_V, Λ_V, t)-*ADS*, where $K_V = N - K_H$ and $\Lambda_V = N - 2K_H + \Lambda_H$.

Accordingly, the coefficients of the interleaved array $w_V(p,q)$ again correspond to an *ADS* arrangement. As a consequence, several properties derived in [28] can be straightforwardly extended. More specifically:

- both sub-arrangements are expected to exhibit low *PSL* values [28];
- each *ADS* pair $\{\mathbf{A}_V, \mathbf{A}_H\}$ can be used to obtain up to $P \times Q$ different interleaved layouts by considering its cyclically-shifted version $\{\mathbf{A}_V^{(\sigma_x,\sigma_y)}, \mathbf{A}_H^{(\sigma_x,\sigma_y)}\}$, with $\mathbf{A}_T^{(\sigma_x,\sigma_y)} \triangleq \{((p+\sigma_x)_{mod\,P}, (q+\sigma_y)_{mod\,Q});\ (p,q) \in \mathbf{A}_T;\ \sigma_x, \sigma_y \in \mathbb{Z}\}$;
- for any aperture size, the computational costs to carry out an array synthesis is negligible [28].

From *Theorem 1*, one can also deduce that the autocorrelation functions of the two arrays are equal except for an offset of $N(1-2\nu)$ ($\nu \triangleq \frac{K_H}{N}$)

$$\xi_V(\tau_x, \tau_y) = \xi_H(\tau_x, \tau_y) + N(1-2\nu) \tag{12}$$

and that, therefore, the corresponding *IDFT*s differ only in the origin of the $k-l$ plane

$$\Xi_V(k,l) = \Xi_H(k,l) + N^2(1-2\nu)\delta(k,l), \tag{13}$$

where $\Xi_V(k,l) \triangleq \sum_{\tau_x=0}^{P-1}\sum_{\tau_y=0}^{Q-1} \xi_V(\tau_x,\tau_y)\exp[2\pi i(\frac{\tau_x k}{P} + \frac{\tau_y l}{Q})]$ [$\xi_V(\tau_x,\tau_y)$ being the autocorrelation function of $\mathbf{A}_V$]. These properties are visually exemplified by the $w_V(p,q)$ and $w_H(p,q)$ blueprints resulting from the $(49, 25, 12, 24)$-*ADS* [43] as well as by the associated autocorrelation functions, which exhibit the predicted three-level behaviour as well as the expected relative shift [Fig. 2(b)].

Notwithstanding the remarked properties of *ADS* interleaved arrangements, a straightforward exploitation of the bounds derived in [28] is not allowed for the considered polarization-agile layout. Indeed, they have been derived for the optimally shifted layouts resulting from $\mathbf{A}_H$ (or $\mathbf{A}_V$) [28]. However, when dealing with interleaved arrangements, it is not generally possible to determine a shift which is optimal for both $\mathbf{A}_H$ and $\mathbf{A}_V$ [31]. Moreover, those bounds apply either to $AF_H(u,v)$ or $AF_V(u,v)$ [28], while, in this case, the properties of the superposition of the two fields taking into account the effects of the element factor [see Eq. (1)] are of interest.

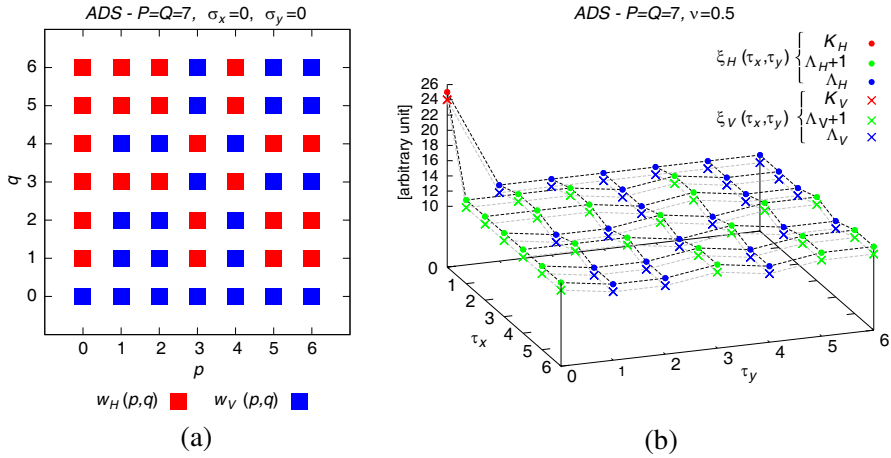

Figure 2. *Mathematical Formulation.* (a) Example of $P = Q = 7$-*ADS* interleaved sequences and (b) associated autocorrelation function.

From the above discussion, it turns out that an extension of the bounds presented in [28] to the considered case is not at hand due to the arbitrary values of α_H, α_V, $\mathbf{EF}_H(u,v)$, and $\mathbf{EF}_V(u,v)$ in Eqs. (1)–(2) and to the requirement to deal with sub-optimal shift values for the *ADS* blueprint pair. Accordingly, a numerical analysis is mandatory to assess the reliability, performances and drawbacks of the considered interleaving scheme for polarization-agile array design.

3. NUMERICAL ANALYSIS

In this section, the results of an extensive numerical study are presented to point out the features, the potentialities, and the limitations of *ADS*s for polarization-agile array design. Towards this end, a set of benchmark *ADS* blueprints with different size and properties are considered. In order to assess the quality of the resulting arrangements, both the arising *PSL* and the polarization purity index Σ[§], defined as

$$\Sigma \triangleq \frac{\int_{R_V} \left[\left|\varepsilon\left(u,v\right) - \varepsilon_D\left(u,v\right)\right| \times S\left(u,v\right)\right] dudv}{Area\left\{R_V\right\}}$$

[R_V being the visible region, and $\varepsilon(u,v)$ being the ellipticity angle of the radiated field [6, 37, 38]] will be analyzed next. In the following,

[§] Σ takes into account the similarity between the desired polarization and the obtained one.

analogously to [6], flanged apertures of size $\frac{\lambda}{2} \times \frac{\lambda}{4}$ excited by the fundamental TE_{10} mode are used as elementary radiators (employing the Fourier transform of the waveguide aperture field for the calculation of $\mathbf{EF}_H(u,v)$ and $\mathbf{EF}_V(u,v)$ [6, 37]), with the larger side disposed along the $\hat{x}$ ($\hat{y}$) axes for the V (H) sub-arrays. Moreover, an inter-element spacing of $s_x = s_y = 0.6\lambda$ is assumed, the steering direction is set to $u_0 = v_0 = \frac{\sqrt{2}}{4}$ (i.e., $\theta_0 = \frac{\pi}{6}$, $\varphi_0 = \frac{\pi}{4}$) [6], and $\varepsilon_D(u,v)$ is chosen as follows

$$\varepsilon_D(u,v) = \begin{cases} -\frac{\pi}{4} & (u,v) \in R \\ \frac{\pi}{4} & \text{otherwise} \end{cases} .$$

Accordingly, a clockwise circular polarization ($\varepsilon_D(u_0,v_0) = -\frac{\pi}{4}$) is enforced in the steering direction by means of (6).

As a first numerical experiment, the performance of the layouts obtained by the $(49, 25, 12, 24)$-*ADS* [43] ($P = Q = 7$, $K_H = 25$, and $K_V = 24$) are analyzed. Fig. 3 describes the behaviour of Σ versus PSL for $\sigma_x = 0, \ldots, P-1$, $\sigma_y = 0, \ldots, Q-1$ as well as the Pareto front of the solution set in the (PSL, Σ) plane. As it can be observed, a set of tradeoffs with $PSL \in [-11.5, -10.5]$ [dB] and $\Sigma \in [0.285, 0.325]$ can be efficiently obtained by a single *ADS* through simple shifts (Fig. 3). The efficiency of the resulting layouts in terms of PSL control are confirmed by the plots of $S(u,v)$ for the six points belonging to the Pareto front (whose layouts are provided in Fig. 8), which show that, although

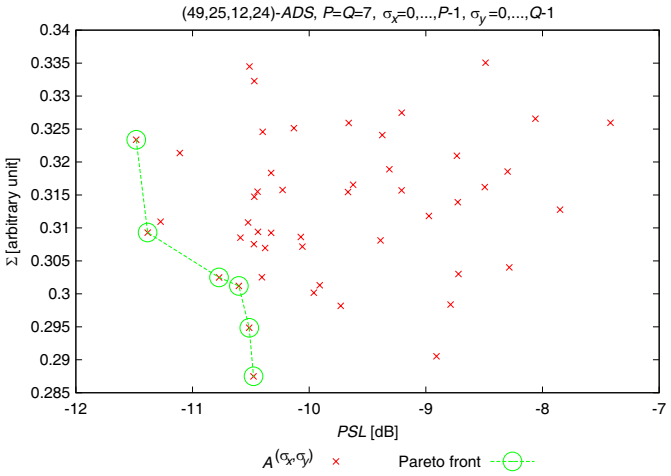

Figure 3. *Numerical assessment* [$P = Q = 7$]. Plots of the representative points of the architectures resulting from the $(49, 25, 12, 24)$-*ADS* in the (Σ, PSL) plane and associated Pareto front.

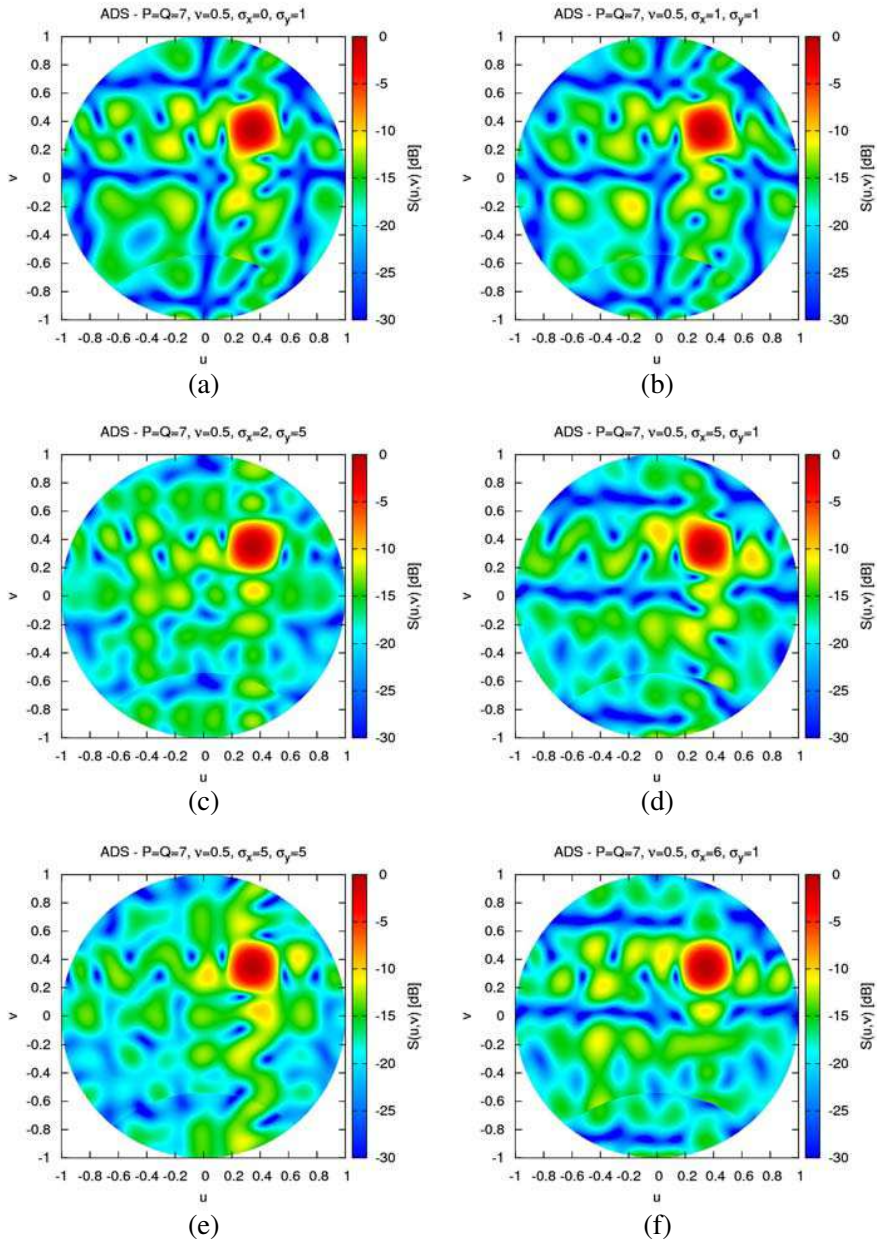

Figure 4. *Numerical assessment* $[P = Q = 7]$. Power patterns of Pareto-optimal layouts resulting from the $(49, 25, 12, 24)$-ADS.

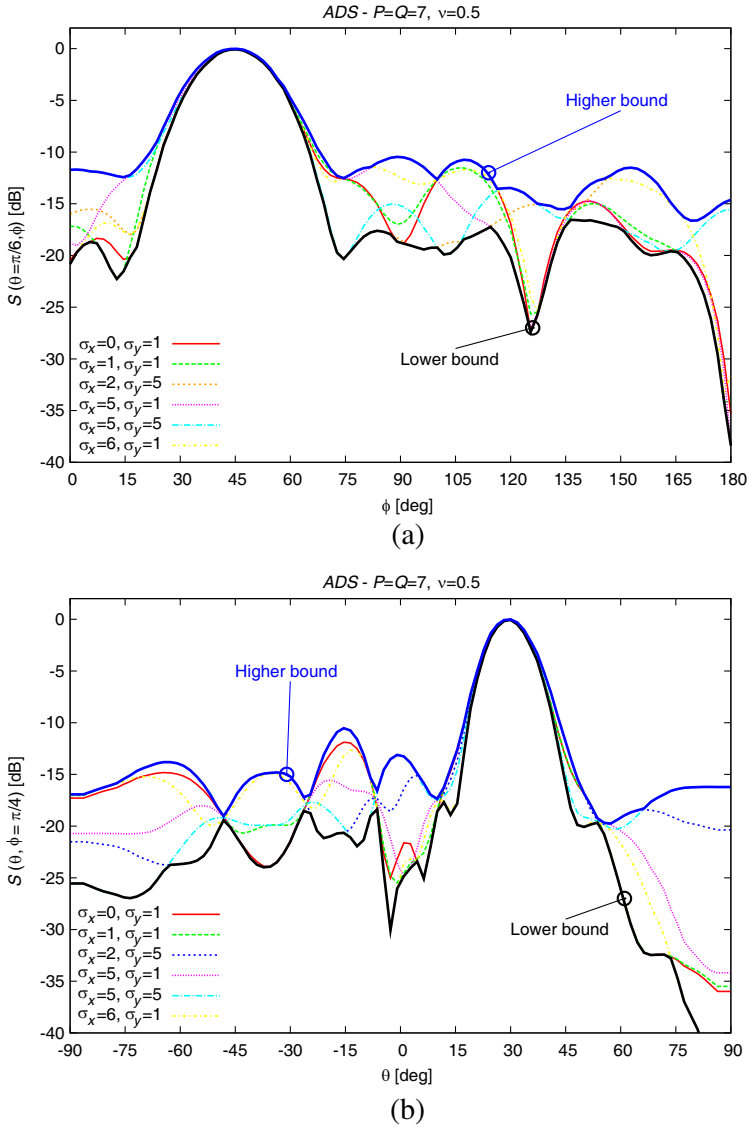

Figure 5. *Numerical assessment* $[P = Q = 7]$. Behaviour of the power patterns of Pareto-optimal layouts resulting from the $(49, 25, 12, 24)$-*ADS* for representative planes: (a) $\theta = \frac{\pi}{6}$; (b) $\varphi = \frac{\pi}{4}$.

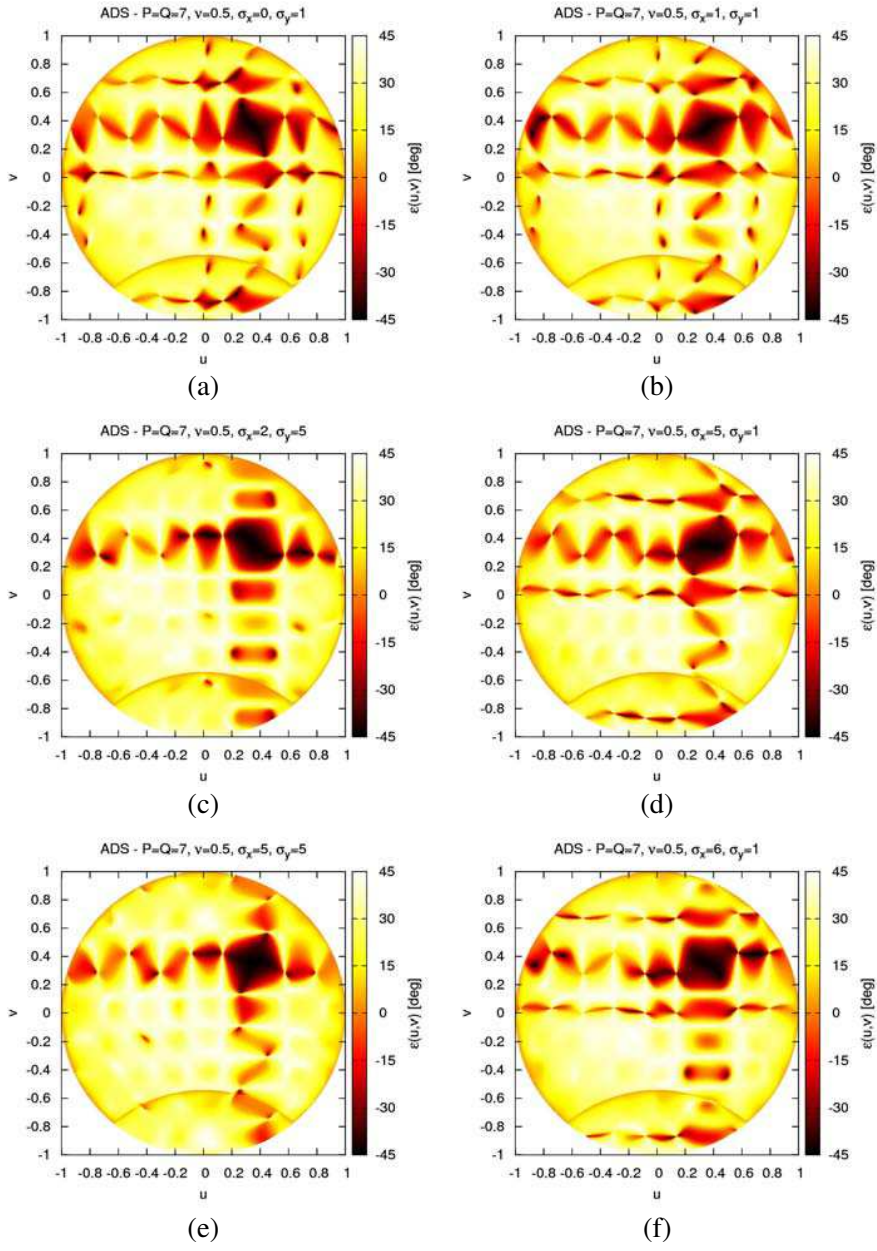

Figure 6. *Numerical assessment* $[P = Q = 7]$. Behaviour of $\varepsilon(u, v)$ for Pareto-optimal layouts resulting from the $(49, 25, 12, 24)$-ADS.

each shift yields a different sidelobe shape, a regular behaviour can be observed for $(u, v) \in R$ in all cases (Fig. 4). Moreover, the radiation patterns in the planes $\varphi = \frac{\pi}{4}$ and $\theta = \frac{\pi}{6}$ (Fig. 5) confirm the absence of grating lobes and the good control of the secondary lobes in the whole visible range [$S(u, v) \lesssim -10.5$ [dB] for $\theta = \frac{\pi}{6}$ — Fig. 5(a) and

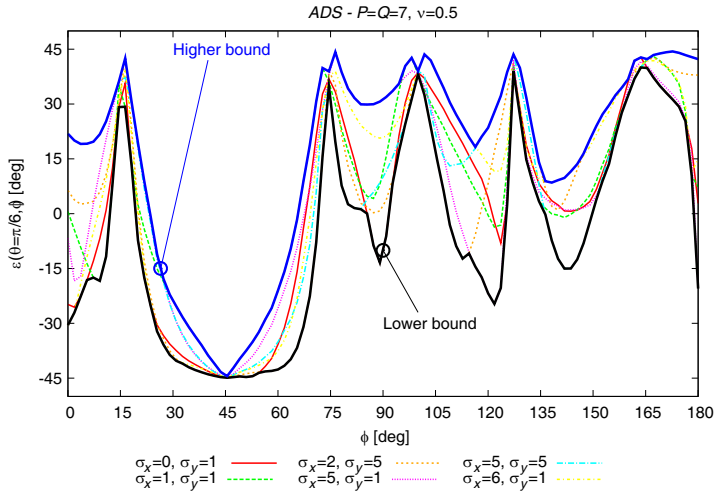

Figure 7. *Numerical assessment* [$P = Q = 7$]. Behaviour of the ellipticity index of Pareto-optimal layouts resulting from the $(49, 25, 12, 24)$-*ADS* for representative planes: (a) $\theta = \frac{\pi}{6}$; (b) $\varphi = \frac{\pi}{4}$.

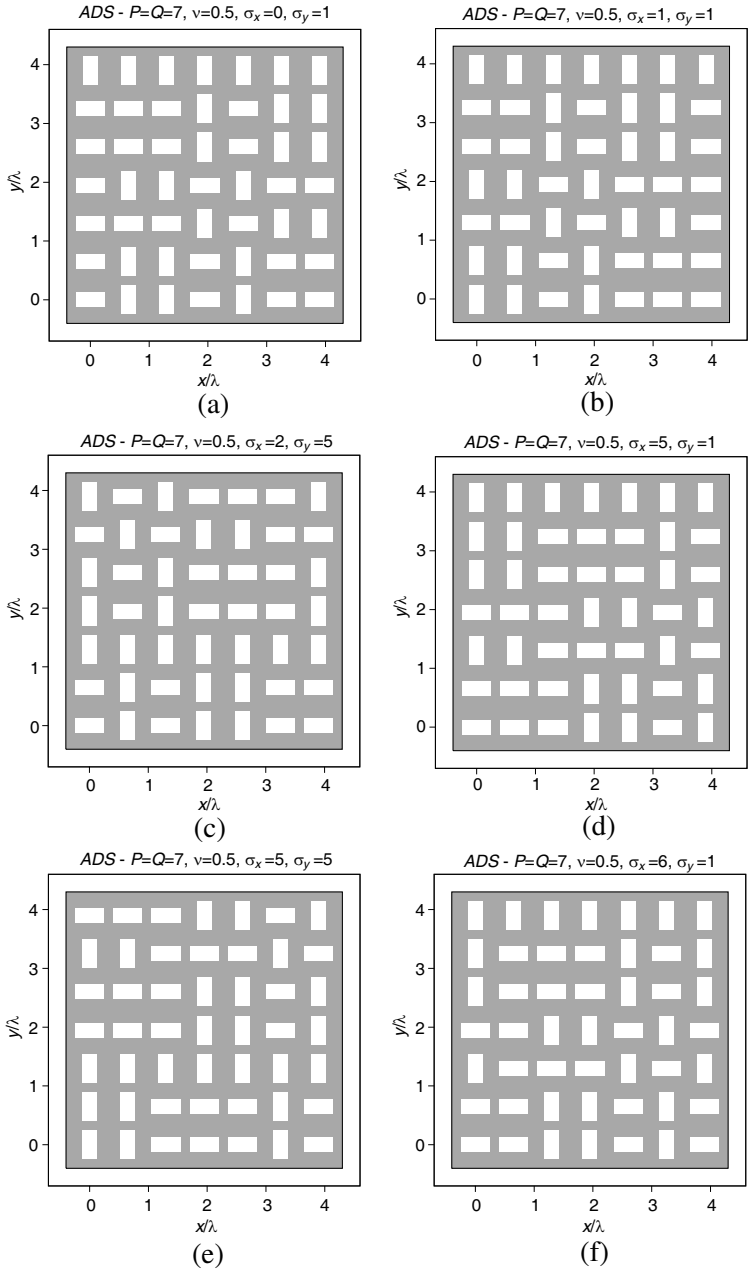

Figure 8. *Numerical assessment* $[P = Q = 7]$. Pareto-optimal architectures resulting from the $(49, 25, 12, 24)$-ADS.

for $\varphi = \frac{\pi}{4}$ — Fig. 5(b)]. As regards the polarization properties of the considered designs, Fig. 6 provides the plots of $\varepsilon(u, v)$ for the *ADS* tradeoff solutions shown in Fig. 4. As it can be noticed, the desired polarization is obtained in the steering direction for all considered tradeoffs ($\varepsilon_D(u_0, v_0) = -\frac{\pi}{4}$ — Fig. 6), while the ellipticity is largely different almost for all angular directions outside R. Moreover, by jointly analyzing the plots of $\varepsilon(u, v)$ with those of $S(u, v)$ (Fig. 6 vs. Fig. 4), it turns out that the (u, v) values in the sidelobe region for

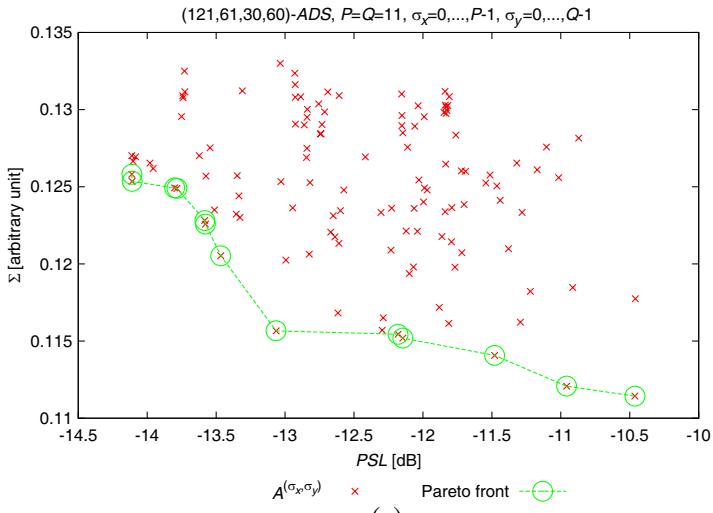

(a)

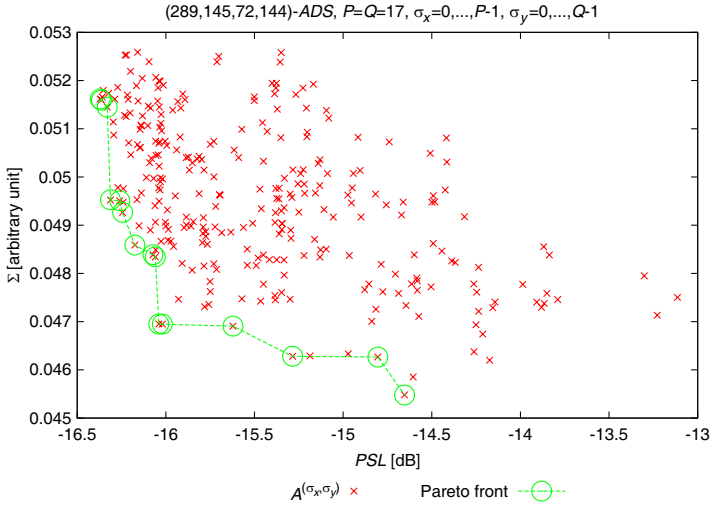

(b)

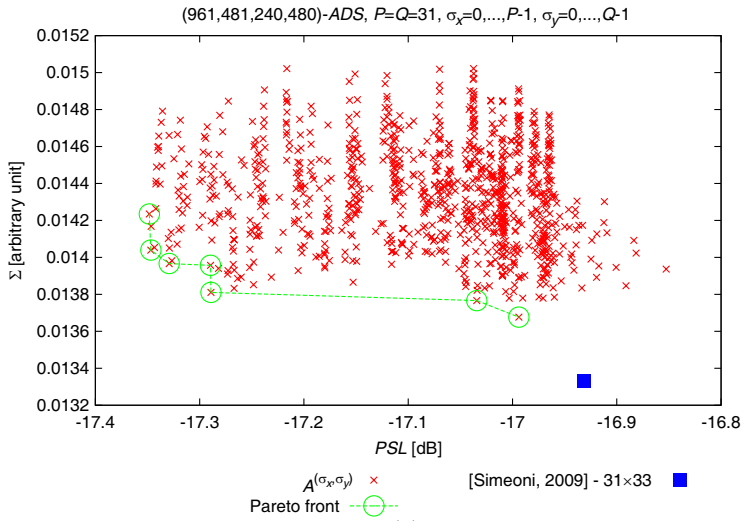

(c)

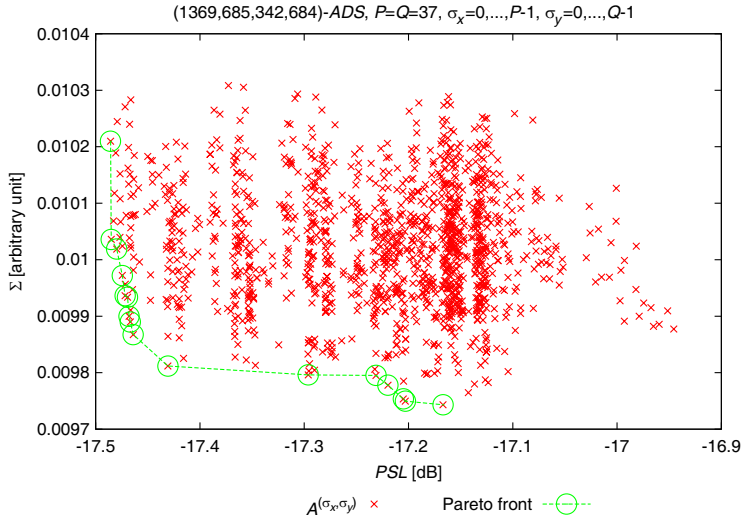

(d)

Figure 9. *Numerical assessment* $[P = Q \in \{11, 17, 31, 37\}]$. Plots of the representative points in the (Σ, PSL) plane and associated Pareto front for the architectures resulting from the (a) $(121, 61, 30, 60)$-ADS, (b) $(289, 145, 72, 144)$-ADS, (c) $(961, 481, 240, 480)$-ADS, and (d) $(1369, 685, 342, 684)$-ADS.

which the ellipticity is close to $-\frac{\pi}{4}$ correspond to low-power directions in the radiation pattern [see for example Fig. 4(e) vs. Fig. 6(e)]. This is even more evident when analyzing the ellipticity index for $\varphi = \frac{\pi}{4}$ [Fig. 7(a)] and $\theta = \frac{\pi}{6}$ [Fig. 7(b)] jointly with Fig. 5: as an example, by considering the behaviour obtained for $\sigma_x = \sigma_y = 1$ in Figs. 5(b) and 7(b) (green line) it results that $\varepsilon(u,v) \approx -\frac{\pi}{4}$ for $\theta \approx \frac{5\pi}{12}$ [Fig. 7(b)], where $S(u,v) < -30$ [dB]. This allows one to conclude that the *ADS* synthesis procedure induces an efficient polarization filtering [6], as it is confirmed by the associated Σ values (Table 1). The layouts associated to the six points belonging to the Pareto front are reported in Fig. 8 for completeness.

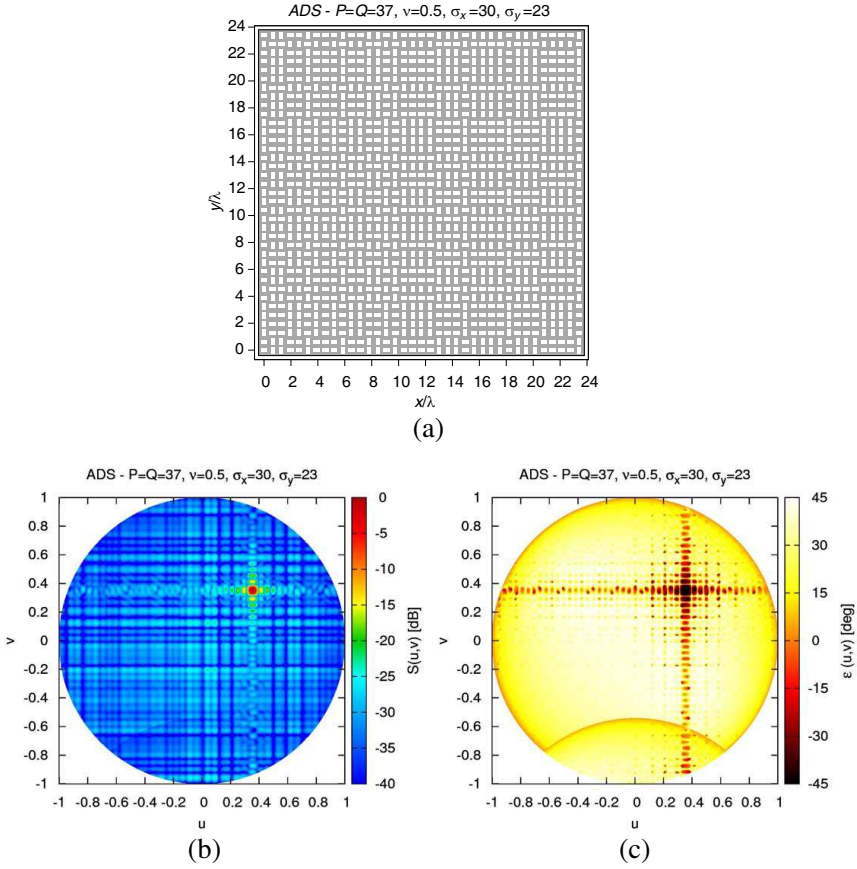

Figure 10. *Numerical assessment* [$P = Q = 37$]. (a) Tradeoff architecture resulting from the $(1369, 685, 342, 684)$-*ADS*, (b) associated power pattern and (c) ellipticity angle.

The effectiveness of *ADS* blueprints for the design of polarization-agile arrays is confirmed by the second set of experiments, dealing with larger values of P and Q (Fig. 9). More specifically, the plots of Σ vs. PSL for the layouts resulting from the $(121, 61, 30, 60)$-*ADS* [Fig. 9(a)], $(289, 145, 72, 144)$-*ADS* [Fig. 9(b)],

Table 1. *Numerical assessment* $[P = Q = 7]$. Array performance indexes for Pareto optimal *ADS* layouts.

Tradeoff			
σ_x	σ_y	PSL [dB]	Σ
0	1	−10.60	0.301
1	1	−10.47	0.287
2	5	−11.48	0.323
5	1	−10.51	0.294
5	5	−11.38	0.309
6	1	−10.77	0.302

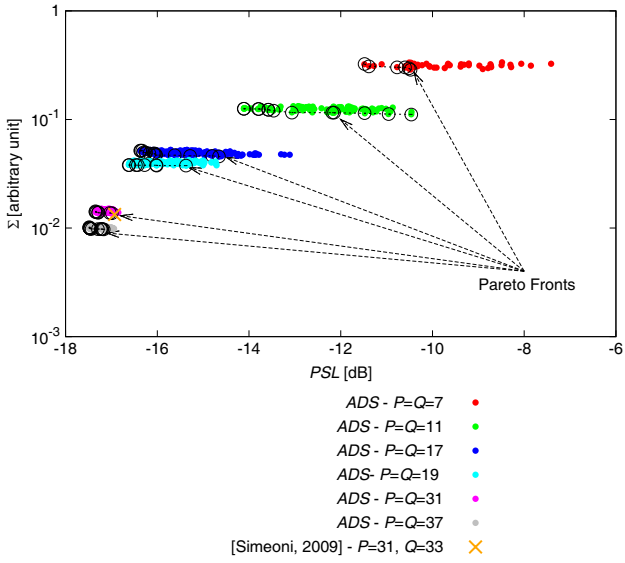

Figure 11. *Numerical assessment.* Comparison of the representative points and Pareto fronts in the (Σ, PSL) plane for *ADS*-based arrays and *DS*-based displacements in [6].

$(961, 481, 240, 480)$-*ADS* [Fig. 9(c)], and $(1369, 685, 342, 684)$-*ADS* [Fig. 9(d)] indicate that both the PSL and the Σ decrease as the array aperture increases [i.e., $\min_{\sigma_x,\sigma_y} PSL\{\mathbf{A}_V^{(\sigma_x,\sigma_y)}, \mathbf{A}_H^{(\sigma_x,\sigma_y)}\} = -14.11$ and $\min_{\sigma_x,\sigma_y} \Sigma\{\mathbf{A}_V^{(\sigma_x,\sigma_y)}, \mathbf{A}_H^{(\sigma_x,\sigma_y)}\} = 0.111$ for $P = Q = 11$ vs. $\min_{\sigma_x,\sigma_y} PSL\{\mathbf{A}_V^{(\sigma_x,\sigma_y)}, \mathbf{A}_H^{(\sigma_x,\sigma_y)}\} = -17.49$ for $P = Q = 37$ and $\min_{\sigma_x,\sigma_y} \Sigma\{\mathbf{A}_V^{(\sigma_x,\sigma_y)}, \mathbf{A}_H^{(\sigma_x,\sigma_y)}\} = 9.74 \times 10^{-3}$, Fig. 9]. Such a behaviour indicates that the sidelobe control as well as the polarization filtering capabilities of *ADS* arrays improve for larger values of $P \times Q$, as

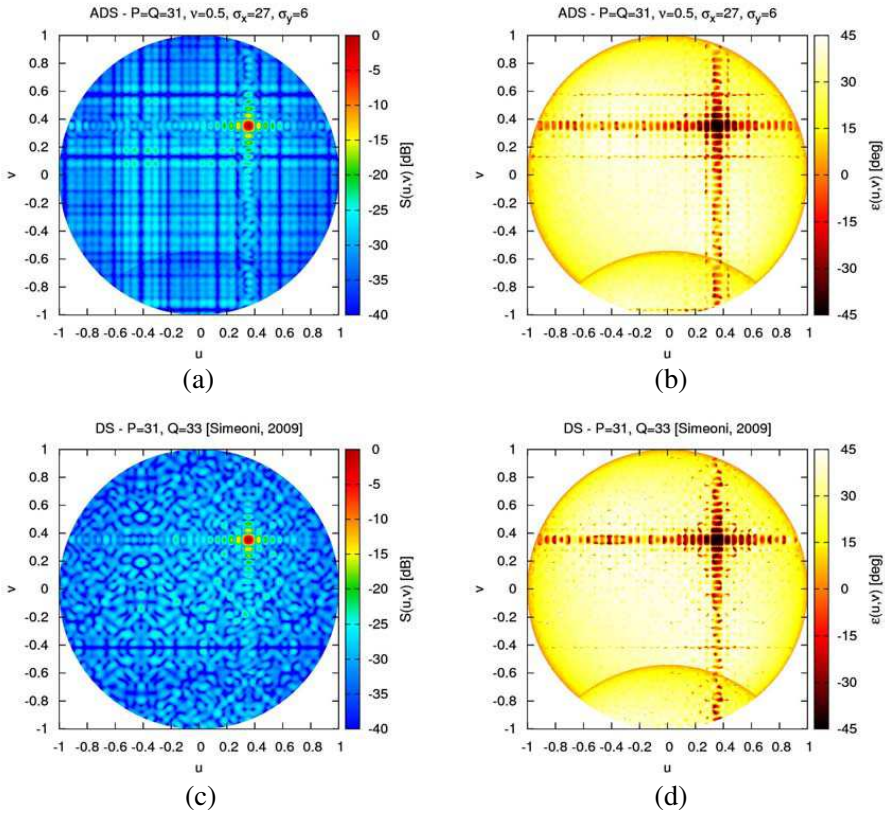

Figure 12. *Numerical assessment* [$P_{DS} = P_{ADS} = 31$, $Q_{DS} = 33$ vs. $Q_{ADS} = 31$]. Behaviour of the radiation pattern and polarization angle of a tradeoff layout resulting from the $(961, 481, 240, 480)$-*ADS* [(a) $S(u)$ and (b) $\varepsilon(u, v)$] and of a reference *DS*-architecture from [6] [(c) $S(u)$ and (d) $\varepsilon(u, v)$].

it can be shown by comparing the plots of $S(u,v)$ [Fig. 10(b)] and $\varepsilon(u,v)$ [Fig. 10(c)] for a selected tradeoff shift in correspondence with $P = Q = 37$ [whose layout is provided in Fig. 10(a)] with those obtained for smaller arrays (Figs. 4 and 6). As a matter of fact, ellipticity values close to $-\frac{\pi}{4}$ are only obtained near $u = u_0$ and $v = v_0$, while an efficient polarization filtering is observed elsewhere, as confirmed by the associated polarization purity index [$\Sigma = 1.02 \times 10^{-2}$]. Moreover, by comparing the Pareto fronts for different PQ values, it is worth observing that larger apertures correspond to smaller variations between the resulting PSLs (Fig. 11). Furthermore, Σ depends significantly on the array size, while in a minor way on the considered shift value (Fig. 11). This suggests that a good polarization

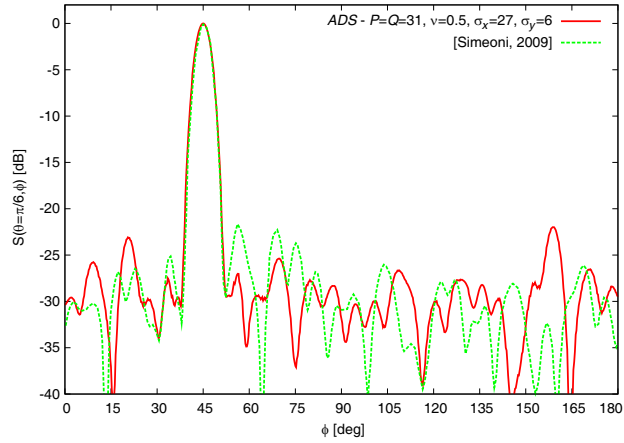

(a)

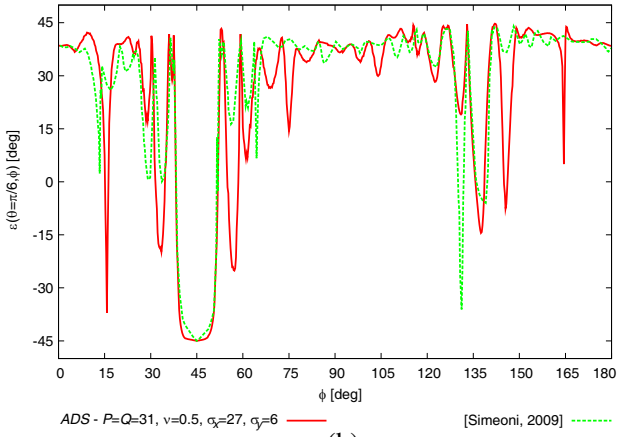

(b)

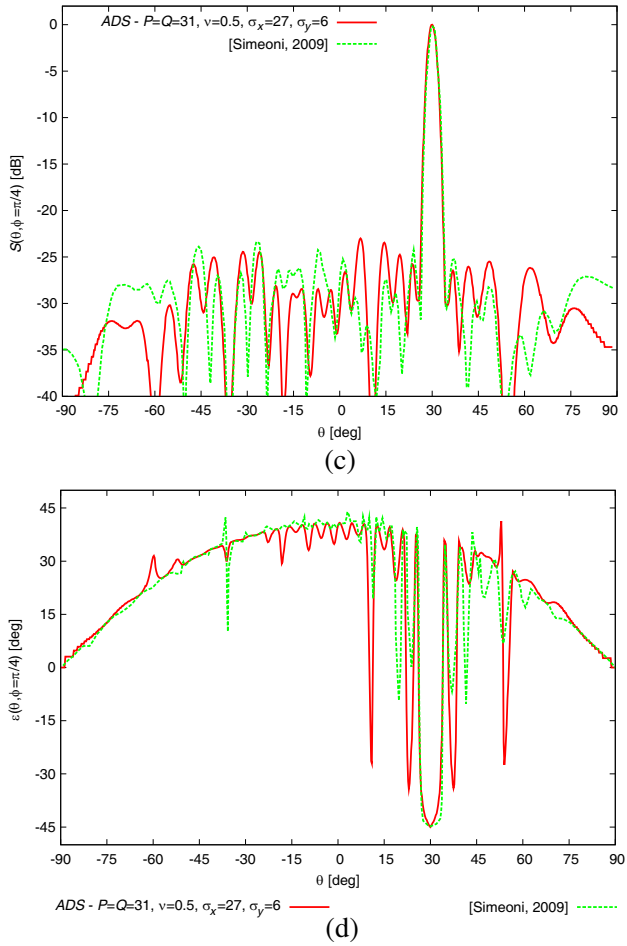

Figure 13. *Numerical assessment* [$P_{DS} = P_{ADS} = 31$, $Q_{DS} = 33$ vs. $Q_{ADS} = 31$]. Behaviour of (a), (c) the radiation pattern and (b), (d) the polarization angle of a tradeoff layout resulting from the $(961, 481, 240, 480)$-*ADS* and of a reference *DS*-architecture from [6] for (a), (b) $\theta = \frac{\pi}{6}$ (c), (d) $\varphi = \frac{\pi}{4}$.

filtering is obtained thanks to the considered *ADS* guideline whatever the employed tradeoff.

In order to complete the analysis of *ADS*-based polarization-agile arrays, a comparison with state-of-the-art techniques is considered. By comparing the behaviour of PSL and Σ for the layout considered

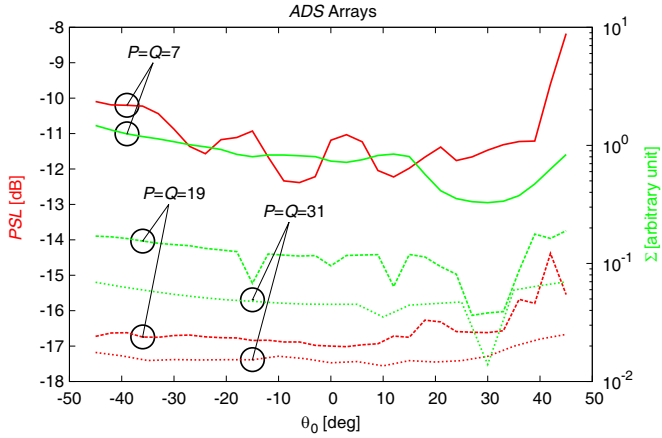

Figure 14. *Numerical assessment* $[\varphi_0 = \frac{\pi}{4}]$. Behaviour of the PSL and Σ versus the steering angle θ_0 for tradeoff layouts resulting from the $(49, 25, 12, 24)$-ADS, $(361, 181, 90, 180)$-ADS, and $(961, 481, 240, 480)$-ADS.

in [6][‖] with those obtained by exploiting the ADS blueprints with roughly the same size $[P_{DS} = P_{ADS} = 31, Q_{DS} = 33$ vs. $Q_{ADS} = 31$ — Fig. 9(c)], it turns out that state-of-the-art DS-based designs provide similar properties with respect to the proposed approach. More specifically, while an improved Σ is allowed by the design in [6] $[\Sigma_{DS} = 1.33 \times 10^{-2}$ vs. $\Sigma_{ADS} \in [1.36 \times 10^{-2}, 1.42 \times 10^{-2}]$ — Fig. 9(c)], lower PSLs are obtained for all tradeoff designs $[PSL_{DS} = -16.93$ [dB] vs. $PSL_{ADS} \in [-17.35, -16.99]$ [dB] — Fig. 9(c)], despite the lower number of elements ($N_{ADS} = 961$ vs. $N_{DS} = 1023$).

The above results are also confirmed by comparing the plots of $S(u, v)$ and $\varepsilon(u, v)$ for the design in [6] [Figs. 12(c) and 12(d)] with those of a selected ADS tradeoff $[\sigma_x = 27, \sigma_y = 6, PSL = -17.28$ [dB], $\Sigma = 1.38 \times 10^{-2}$ — Figs. 12(a) and 12(b)]. Indeed, very similar properties are obtained both in terms of sidelobe control [Fig. 12(a) vs. Fig. 12(c)] and of polarization filtering capabilities [Fig. 12(b) vs. Fig. 12(d)]. The similarity is even more evident from the plots of the radiated power and of the ellipticity angle for two representative planes [$\theta = \frac{\pi}{6}$ — Figs. 13(a), Fig. 13(b); $\varphi = \frac{\pi}{4}$ — Figs. 13(c), Fig. 13(d)] which indicate that the performances of DS and ADS layouts only marginally differ in terms of sidelobe control [Figs. 13(a), 13(c)]. Moreover, it is worth noticing that ellipticity values close to $-\frac{\pi}{4}$

[‖] The numerical simulations have been carried out considering the elementary radiators, element spacing and size of [6].

outside the mainlobe correspond in both cases to low-power directions in the radiation pattern [Figs. 13(b), 13(d)].

As a final numerical experiment, the mutual coupling between the individual elements is taken into account to evaluate its effects on *ADS*-based polarization agile layouts. Towards this end, a numerical simulation of the architecture considered in Fig. 8(c) ($P = Q = 7$) has been carried out by using a *MoM*-based full-wave solver, and evaluating the arising radiation pattern $S_{MoM}(u, v)$ and ellipticity index $\varepsilon_{MoM}(u, v)$ again considering flanged apertures as elementary antennas. From the plots of $S_{MoM}(u, v)$ [Fig. 14(a)] and $S(u, v)$ [Fig. 4(c)] it turns out that the presence of mutual coupling affects the array pattern behaviour in the sidelobe region, therefore inducing a higher PSL ($PSL_{MoM} \approx -4.10\,[\text{dB}]$ vs. $PSL = -11.48\,[\text{dB}]$). However, when observing the behaviour of the radiated power for selected planes [$\theta = \frac{\pi}{6}$ — Fig. 15(a); $\varphi = \frac{\pi}{4}$ — Fig. 15(b)] it can be noticed that the increase of the sidelobe radiation due to mutual coupling does not lead to grating lobes in all cases. As far as the polarization properties are concerned, the plots of $\varepsilon_{MoM}(u, v)$ and $\varepsilon(u, v)$ in selected planes [$\theta = \frac{\pi}{6}$ — Fig. 15(b); $\varphi = \frac{\pi}{4}$ — Fig. 15(c)] indicate that the ellipticity angle distortion due to mutual coupling is marginal near the steering direction, while it becomes stronger in the sidelobe region. However, it is worth observing that $\varepsilon_{MoM}(u, v) \to -\frac{\pi}{4}$ in the sidelobe region when $S_{MoM}(u, v) < -20\,[\text{dB}]$ [Fig. 15(d) vs. Fig. 15(c)]. This indicates that the overall polarization filtering capability of the proposed layout is not significantly affected by the

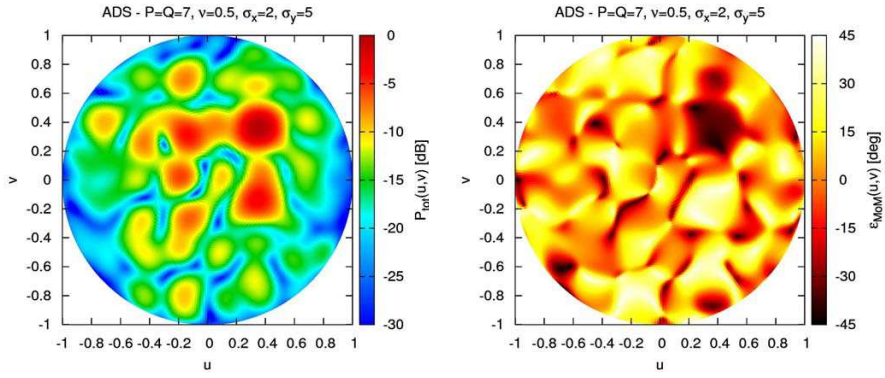

(a) (b)

Figure 15. *Numerical assessment* [$P = Q = 7$-*MoM simulations*]. Behaviour of (a) $S_{MoM}(u, v)$ and (b) $\varepsilon_{MoM}(u, v)$ for a tradeoff layout resulting from the $(49, 25, 12, 24)$-*ADS*.

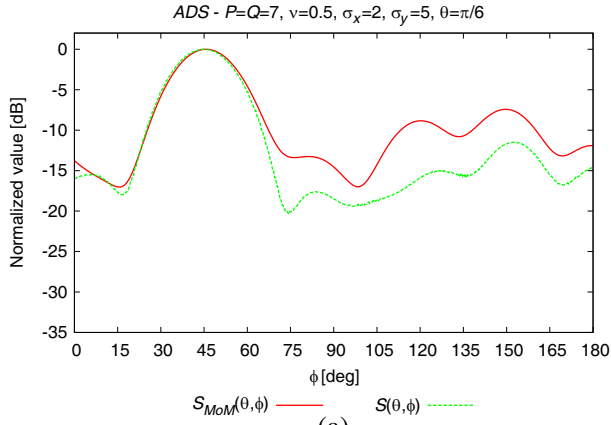
ADS - P=Q=7, ν=0.5, σx=2, σy=5, θ=π/6
Normalized value [dB]
0
-5
-10
-15
-20
-25
-30
-35
0 15 30 45 60 75 90 105 120 135 150 165 180
ϕ [deg]
SMoM(θ,ϕ)
S(θ,ϕ)

(a)

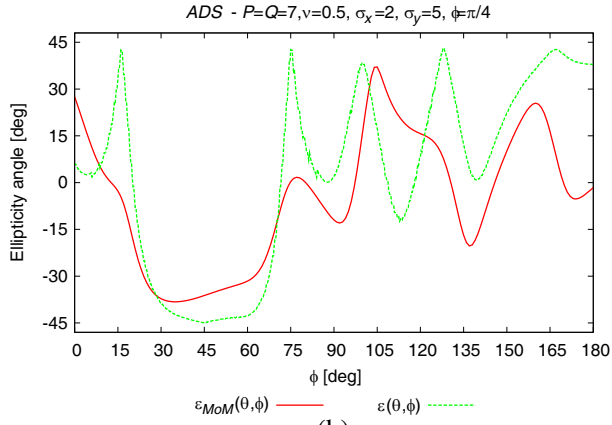
ADS - P=Q=7,ν=0.5, σx=2, σy=5, ϕ=π/4
Ellipticity angle [deg]
45
30
15
0
-15
-30
-45
0 15 30 45 60 75 90 105 120 135 150 165 180
ϕ [deg]
εMoM(θ,ϕ)
ε(θ,ϕ)

(b)

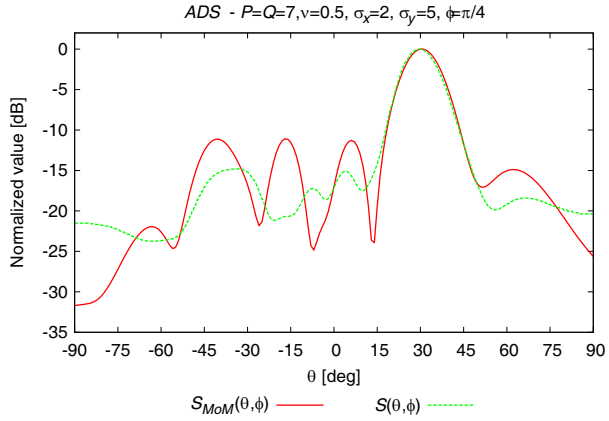
ADS - P=Q=7,ν=0.5, σx=2, σy=5, ϕ=π/4
Normalized value [dB]
0
-5
-10
-15
-20
-25
-30
-35
-90 -75 -60 -45 -30 -15 0 15 30 45 60 75 90
θ [deg]
SMoM(θ,ϕ)
S(θ,ϕ)

(c)

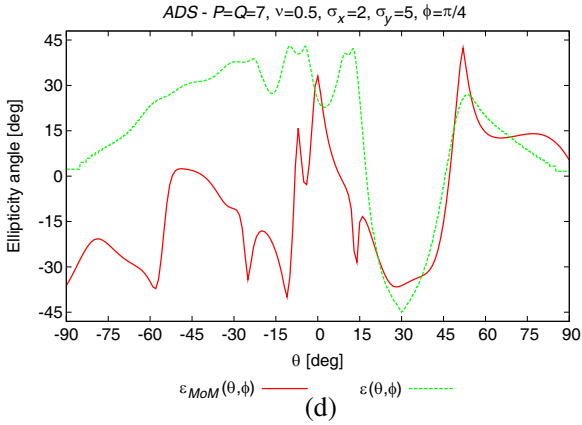

Figure 16. *Numerical assessment* [$P = Q = 7$-MoM *simulations*]. Comparison of (a), (c) the radiation pattern and (b), (d) the polarization angle in the presence (red lines) or absence (green lines) of mutual coupling for a tradeoff layout based on the $(49, 25, 12, 24)$-ADS: (a), (b) $\theta = \frac{\pi}{6}$ (c), (d) $\varphi = \frac{\pi}{4}$.

presence of mutual coupling, as it is confirmed by comparing the plots of $\varepsilon_{MoM}(u, v)$ [Fig. 14(b)] and $\varepsilon(u, v)$ [Fig. 6(c)] in the whole visible range.

4. CONCLUSIONS

In this paper, an ADS-based methodology has been proposed to design arrays with polarization-agile features. The method relies on the interleaving of two independently polarized sub-arrays with different feeding amplitudes and phases. The properties of ADS-based layouts are exploited in order to guarantee a good PSL control whatever the desired polarization state. An extensive numerical validation has been carried out to assess the feasibility and reliability of the proposed ADS methodology as well as the arising PSL and polarization filtering performances. Moreover, selected numerical simulations aimed at comparing the proposed methodology with state-of-the-art approaches have been presented. Furthermore, the effects of mutual coupling between the array elements have been evaluated by means of full-wave simulations. The obtained results have pointed out that

- each ADS blueprint can be exploited to synthesize a set of tradeoff polarization-agile arrangements with negligible computational efforts;

- improved sidelobe control and polarization filtering performances can be obtained when enlarging the array aperture;
- *ADS* layouts favorably compare with state-of-the-art *DS* designs in terms of *PSL* and Σ performances, and they are available for a wider set of descriptive parameters;
- the polarization filtering capabilities of *ADS* layouts are only negligibly affected by the presence of mutual coupling, while higher *PSL* values are obtained when such effects are taken into account;
- analogously to [6], the proposed architecture has several realization advantages with respect to standard polarization agile architectures relying on reconfigurable array elements;
- the *ADS* blueprints can be used as a starting point for a local or global optimization procedure in order to improve their rate of convergence.

Future efforts will be aimed at providing *a-priori* estimates of the polarization filtering and *PSL* performances of interleaved arrangements based on *ADS* sequences, as well as the analysis of suitable countermeasures to mutual coupling effects, including the design of ad-hoc elementary radiators for the "*H*" and "*V*" sub-arrays. Finally, although out-of-the-scope of this paper and related to combinatorial mathematics, advances in *ADS* generation techniques are expected.

ACKNOWLEDGMENT

The authors wish to thank Prof. Douglas H. Werner for his valuable comments and suggestions.

REFERENCES

1. Soliman, E. A., W. De Raedt, and G. A. E. Vandenbosch, "Reconfigurable slot antenna for polarization diversity," *Journal of Electromagnetic Waves and Applications*, Vol. 23, No. 7, 905–916, 2009.
2. Alkanhal, M. and A. F. Sheta, "A novel dual-band reconfigurable square-ring microstrip antenna," *Progress In Electromagnetics Research*, Vol. 70, 337–349, 2007.
3. Nolen, J., "Phased array polarization agility," *IEEE Trans. Antennas Propag.*, Vol. 13, No. 5, 820–821, 1965.
4. Giuli, D., "Polarization diversity in radar," *Proc. IEEE*, Vol. 74, No. 2, 245–269, 1986.

5. Gao, S., A. Sambell, and S. S. Zhong, "Polarization-agile antennas," *IEEE Antennas Propagat. Mag.*, Vol. 48, No. 3, 28–37, 2006.
6. Simeoni, M., I. E. Lager, C. I. Coman, and A. G. Roeder, "Implementation of polarization agility in planar phased-array antennas by means of interleaved subarrays," *Radio Sci.*, Vol. 44, RS5013, 1–26, 2009.
7. Skolnik, M. I., *Introduction to Radar Systems*, 2nd Edition, McGraw-Hill, New York, 1981.
8. Shaubert, D. H., F. C. Farrar, A. Sindoris, and S. T. Hayes, "Microstrip antennas with frequency agility and polarization diversity," *IEEE Trans. Antennas Propag.*, Vol. 29, No. 1, 118–123, Jan. 1981.
9. Korosec, T., P. Ritos, and M. Vidmar, "Varactor-tuned microstrip-patch antenna with frequency and polarisation agility," *Electron. Lett.*, Vol. 42, No. 18, 7–8, 2006.
10. Wei, W.-B., Q.-Z. Liu, Y.-Z. Yin, and H.-J. Zhou, "Reconfigurable microstrip patch antenna with switchable polarization," *Progress In Electromagnetics Research*, Vol. 75, 63–68, 2007.
11. Chen, Y. B., T. B. Chen, Y. C. Jiao, and F. S. Zhang, "A reconfigurable microstrip antenna with switchable polarization," *Journal of Electromagnetic Waves and Applications*, Vol. 20, No. 10, 1391–1398, 2006.
12. Xu, H.-X., G.-M. Wang, and M.-Q. Qi, "A miniaturized triple-band metamaterial antenna with radiation pattern selectivity and polarization diversity," *Progress In Electromagnetics Research*, Vol. 137, 275–292, 2013.
13. Vongsack, S., C. Phongcharoenpanich, S. Kosulvit, K. Hamamoto, and T. Wakabayashi, "Unidirectional antenna using two-probe excited circular ring above square reflector for polarization diversity with high isolation," *Progress In Electromagnetics Research*, Vol. 133, 159–176, 2013.
14. Zhao, Y.-L., C. Gai, L. Liu, J.-P. Xiong, J. Chen, and Y.-C. Jiao, "Novel polarization reconfigurable annular ring-slot antenna," *Journal of Electromagnetic Waves and Applications*, Vol. 22, Nos. 11–12, 1587–1592, 2008.
15. Sun, L., B.-H. Sun, J.-Y. Li, Y.-H. Huang, and Q.-Z. Liu, "Reconfigurable dual circularly polarized microstrip antenna without orthogonal feeding network," *Journal of Electromagnetic Waves and Applications*, Vol. 25, No. 10, 1352–1359, 2011.

16. Biffi Gentili, G. and C. Salvador, "New serially fed polarisation-agile linear array of patches," *IEE Proc. Microw. Antennas Propag.*, Vol. 145, No. 5, 392–396, Oct. 1998.
17. Zhong, S.-S., X.-X. Yang, and S.-C. Gao, "Polarization-agile microstrip antenna array using a single phase-shift circuit," *IEEE Trans. Antennas Propag.*, Vol. 52, No. 1, 84–87, 2004.
18. Yen, S.-C. and T.-H. Chu, "A beam-scanning and polarization agile antenna array using mutually coupled oscillating doublers," *IEEE Trans. Antennas Propag.*, Vol. 53, No. 12, 4051–4057, Dec. 2005.
19. Huang, J., "A technique for an array to generate circular polarization with linearly polarized elements," *IEEE Trans. Antennas Propagat.*, Vol. 34, No. 9, 1113–1124, 1986.
20. Coman, C. I., I. E. Lager, and L. P. Ligthart, "The design of shared aperture antennas consisting of differently sized elements," *IEEE Trans. Antennas Propag.*, Vol. 54, No. 2, 376–383, 2006.
21. Oliveri, G., P. Rocca, and A. Massa, "Interleaved linear arrays with difference sets," *Electron. Lett.*, Vol. 45, No. 5, 323–324, 2010.
22. Oliveri, G., F. Caramanica, C. Fontanari, and A. Massa, "Rectangular thinned arrays based on McFarland difference sets," *IEEE Trans. Antennas Propag.*, Vol. 59, No. 5, 1546–1552, May 2011.
23. Leeper, D. G., "Isophoric arrays — Massively thinned phased arrays with well-controlled sidelobes," *IEEE Trans. Antennas Propag.*, Vol. 47, No. 12, 1825–1835, Dec. 1999.
24. Oliveri, G., M. Donelli, and A. Massa, "Genetically-designed arbitrary length almost difference sets," *Electron. Lett.*, Vol. 45, No. 23, 1182–1183, Nov. 2009.
25. Arasu, K. T., C. Ding, T. Helleseth, P. V. Kumar, and H. M. Martinsen, "Almost difference sets and their sequences with optimal autocorrelation," *IEEE Trans. Inf. Theory*, Vol. 47, No. 7, 2934–2943, Nov. 2001.
26. Zhang, Y., J. G. Lei, and S. P. Zhang, "A new family of almost difference sets and some necessary conditions," *IEEE Trans. Inf. Theory*, Vol. 52, No. 5, 2052–2061, May 2006.
27. Oliveri, G., M. Donelli, and A. Massa, "Linear array thinning exploiting almost difference sets," *IEEE Trans. Antennas Propag.*, Vol. 57, No. 12, 3800–3812, Dec. 2009.
28. Oliveri, G., L. Manica, and A. Massa, "ADS-based guidelines for thinned planar arrays," *IEEE Trans. Antennas Propag.*, Vol. 58, 1935–1948, Jun. 2010.

29. Oliveri, G., L. Manica, and A. Massa, "On the impact of mutual coupling effects on the PSL of ADS thinned arrays," *Progress In Electromagnetic Research B*, Vol. 17, 293–308, 2009.
30. Carlin, M., G. Oliveri, and A. Massa, "On the robustness to element failures of linear ADS-thinned arrays," *IEEE Trans. Antennas Propag.*, Vol. 59, No. 12, 4849–4853, Dec. 2011.
31. Oliveri, G. and A. Massa, "Fully-interleaved linear arrays with predictable sidelobes based on almost difference sets," *IET Radar, Sonar & Navigation*, Vol. 4, No. 5, 649–661, Oct. 2010.
32. Oliveri, G. and A. Massa, "ADS-based array design for 2D and 3D ultrasound imaging," *IEEE Trans. on Ultrason., Ferroelectr., and Freq. Control*, Vol. 57, No. 7, 1568–1582, Jul. 2010.
33. Oliveri, G., F. Caramanica, M. D. Migliore, and A. Massa, "Synthesis of non-uniform MIMO arrays through combinatorial sets," *IEEE Antennas Wireless Propag. Lett.*, Vol. 11, 728–731, 2012.
34. Oliveri, G. and A. Massa, "Genetic algorithm (GA)-enhanced almost difference set (ADS)-based approach for array thinning," *IET Microw. Antennas Propag.*, Vol. 5, No. 3, 305–315, Feb. 2011.
35. Oliveri, G., F. Caramanica, and A. Massa, "Hybrid ADS-based techniques for radio astronomy array design," *IEEE Trans. Antennas Propag.*, Vol. 59, No. 6, 1817–1827, Jun. 2011.
36. Mailloux, R. J., *Phased Array Antenna Handbook*, Artech House, Inc., Norwood, MA, 2005.
37. Balanis, C. A., *Antenna Theory: Analysis and Design*, 2nd Edition, Wiley, New York, 1997.
38. Kraus, J. D., *Antennas*, 2nd edition, McGraw Hill, New York, 1988.
39. MacWilliams, F. J. and N. J. Sloane, "Pseudo random sequences and arrays," *Proc. IEEE*, Vol. 64, No. 12, Dec. 1976.
40. McFarland, R. J., "A family of difference sets in non-cyclic groups," *Journal of Combinatorial Theory A*, Vol. 15, No. 1, 1–10, Jul. 1973.
41. Turyn, R. J., "Character sum and difference sets," *Pacific J. Math.*, Vol. 15, No. 1, 319–346, 1965.
42. La Jolla Cyclic Difference Set Repository, http://www.ccrwest.org/diffsets.html.
43. ELEDIA Almost Difference Set Repository, http://www.eledia.ing.unitn.it/.